High Bulk Electron Mobility Diketopyrrolopyrrole Copolymers with Perfluorothiophene

*Christian J. Mueller, Chetan R. Singh, Martina Fried, Sven Huettner, and Mukundan Thelakkat**

The question of designing high electron mobility polymers by increasing the planarization using diffusive nonbonding heteroatom interactions in diketopyrrolopyrrole polymers is addressed in this. For this, three different diketopyrrolo[3,4-*c*]pyrrole (DPP) derivatives with thienyl-, 2-pyridinyl-, and phenyl-flanked cores are copolymerized with an electron-rich thiophene unit as well as an electron-deficient 3,4-difluorothiophene unit as comonomer to obtain diverse polymeric DPPs which vary systematically in their structures. The crystallinity differs significantly with clear trends on varying both flanking unit and comonomer. The optical gap and energy levels depend more on the nature of the flanking aryl units rather than on fluorination. Additionally, the charge transport properties are compared using different methods to differentiate between interface or orientation effects and bulk charge carrier transport. In organic field effect transistor devices with very high electron as well as hole mobilities (up to 0.6 $cm^2 V^{-1} s^{-1}$) are obtained and fluorination leads to a more pronounced n-type nature in all polymers, resulting in ambipolar behavior in otherwise p-type materials. In contrast, space-charge limited current measurements show a strong influence of the flanking units only on electron mobilities. Especially, the elegant synthetic strategy of combining pyridyl flanking units with difluorothiophene as the comonomer culminates in a record bulk electron mobility of 4.3×10^{-3} $cm^2 V^{-1} s^{-1}$ in polymers.

1. Introduction

Diketopyrrolo[3,4-*c*]pyrrole (DPP) based polymer materials are promising candidates for organic field effect transistors (OFET) as well as organic photovoltaics (OPV) due to their high ambipolar charge carrier mobilities, low optical gap and high absorption coefficient.[1] Most reports focus on DPP polymers (PDPP) as donor materials in OPV, which show high power conversion efficencies (PCE) when blended with a C_{60} or C_{70} fullerene derivative (PCBM).[1a,2] Usually, the bicyclic DPP core is flanked on both sides with aryl units, such as thiophene, phenyl, or pyridine groups. This diaryl-DPP is usually copolymerized using a variety of comonomers containing phenyl, thiophene, or thienothiophene moieties.[1c,3] The copolymers are synthesized using either Suzuki or Stille polycondensation. Among the vast variety of DPP copolymers, PDPP3T having thiophene as both flanking aryl units and comonomer is widely studied in a variety of devices.[3a,4]

The charge carrier mobility of different PDPPs has been usually investigated in OFET devices. Hole and electron mobilities, in some of these materials are high in the range of about 10^{-2} to 10^{1} $cm^2 V^{-1} s^{-1}$, especially after thermal treatment of the thin films.[1d,5] This is mainly due to the high crystallinity of these tested PDPPs which favors ordered packing with possible orientation effects on annealing. It has been reported, that thermal annealing in some PDPPs leads to the formation of a preferentially edge-on orientation at the semiconductor–dielectric interface, causing these high mobilities.[6] Thus, OFET mobilities give more insight into orientation effects at the interface, as charge carriers are transported within a narrow channel of 5–10 nm of the semiconducting layer. Even though this is very relevant for charge injection or collection at the electrode interface, it is very necessary to evaluate and understand the bulk charge carrier mobility of PDPPs as measured in a diode configuration. Here, charge carriers are transported vertically through the active layer over more than 100 nm, which is similar to thicknesses in solar cells. Moreover, there is a considerable difference in the charge-carrier density present in the OFET and diode configurations.[7] For PDPPs space-charge limited current (SCLC) measurements in diode geometry are mainly reported in PDPP:PCBM blends. For determination of the hole-mobility (μ_h) of PDPP this is an acceptable experimental simplification since the contribution of fullerene to μ_h is negligible. Electron mobilities (μ_e), however, cannot be assessed in the blended material, since fullerenes contribute considerably to the electron transport.

One of the main questions of concern is the design and development of efficient electron transport polymer materials. In the case of DPP derivatives new heteroaromatic units have recently been attached to the DPP core to improve the acceptor nature of these materials. For example, Janssen et al. employed thiazole flanking units to provide n-type polymers that have successfully been used in all-polymer OPV as an acceptor material.[8]

C. J. Mueller, Dr. C. R. Singh, M. Fried, Prof. S. Huettner, Prof. M. Thelakkat
Applied Functional Polymers – Macromolecular Chemistry I
University of Bayreuth
95440 Bayreuth, Germany
E-mail: mukundan.thelakkat@uni-bayreuth.de

DOI: 10.1002/adfm.201404540

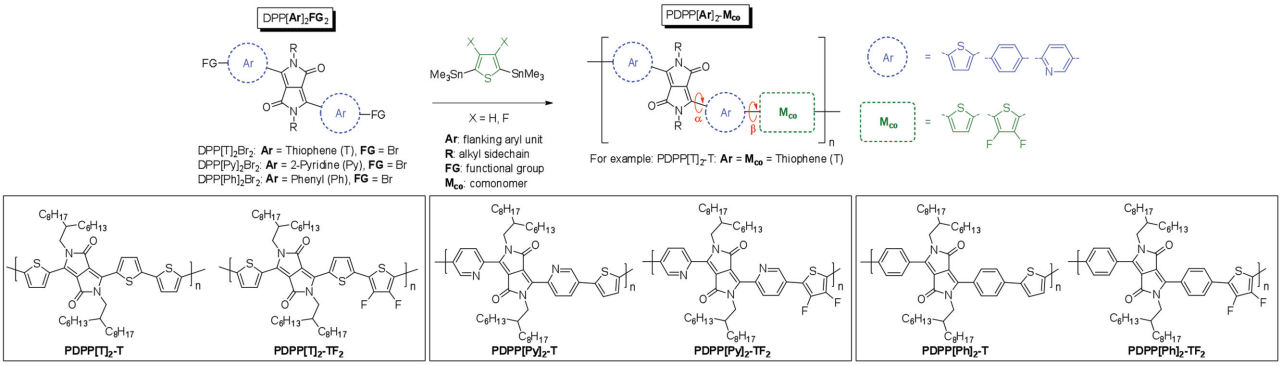

Scheme 1. Synthesis of the PDPP copolymers using $Pd_2(dba)_3/P(o\text{-}Tol)_3$ in chlorobenzene at 180 °C in a microwave reactor. All polymers were end-capped with 2-tributyltinthiophene and 2-bromothiophene. The modular nomenclature approach for DPP monomers and polymers is shown with the two dihedral angles of interest α and β depicted in the polymer structure.

Another general approach is to use fluorinated moieties to tune energy levels to obtain suitable donor or acceptor materials.[6,9]

Both absorption and charge carrier mobility of polymers are dependent on the degree of delocalization and hence planarity of the conjugated polymer backbone.[10] Recently, it has been published and backed by a number of theoretical calculations that the planarity of backbones in conjugated polymer can be increased via diffusive nonbonding heteroatom interactions.[11] In addition to the classical S–O interactions, most importantly CH–N, CH–O, CH–F, and CH–S interactions of adjacent aryl units can contribute to a rigidification of the polymer chain. For PDPPs there are two options for modification of the backbone in order to increase the planarity. The aryl units **Ar** adjacent to the diketopyrrolo[3,4-*c*]pyrrole core can be altered in order to modify both of the dihedral angles α and β (see **Scheme 1**). Generally, PDPPs employing phenyl flanking units show only modest charge carrier mobilites in OFET devices and poor power conversion efficiencies in OPVs when blended with fullerene acceptors.[12] This poor performance is mostly ascribed to the large dihedral angle between the bicyclic DPP core and the phenyl groups as flanking aromatic units.[13] In contrast, most of the thienyl-flanked PDPPs exhibit high charge carrier mobilities as well as high PCEs in OPV devices. This is not only due to a more favorable, coplanar structure but also due to effective orbital overlap that profits from a push–pull-effect of the DPP core and thiophene flanking units, which lowers the optical gap of the material. When 2-pyridine, which lacks the hydrogen atom at 2-position, is used instead of the phenyl-unit, the steric hindrance between the keto-group in the DPP core and the 2-hydrogen-position (vacant) of the adjacent aryl ring as well as any steric interaction between the 6-hydrogen pyridine and $N–CH_2$ of the alkyl chain can be avoided in appropriate conformations. Whereas thiophene is a very electron rich unit, pyridine is comparatively electron deficient, allowing for the design of electron-transporting materials. For example, the copolymer, which consists of pyridine flanked DPP and 2,2′-bithiophene as comonomers, showed extremely high electron mobility in the range of 6 $cm^2\ V^{-1}\ s^{-1}$ in OFET devices.[14]

The second option is the modification of the comonomer $\mathbf{M_{co}}$ in order to optimize the dihedral angle β. A versatile way of fixing this dihedral angle between the diaryl-DPP and the comonomer is the exploitation of the aforementioned diffusive interactions. Substitution of aromatic hydrogen atoms in the comonomer with fluorine gives rise to CH–F coordination sites and electron-deficient comonomers. This fluorination approach has been demonstrated using fluorinated units for the development of semiconducting polymers relevant to both OFET as well as OPV devices.[6,15] Ladder-type comonomers with up to five multifused aromatic rings sterically locked by covalent bridging have also been employed.[16] However, even if these comonomers are very rigid for themselves, the dihedral angle β cannot be minimized by this approach.

Complex applications such as photovoltaics demand a combination of optimum absorption, crystallinity, and bulk charge carrier transport at the same time. In order to achieve all these simultaneously a comprehensive picture of how structural variation affects the individual properties is required. This can be obtained only by a gradual structural variation and by comparatively studying its influences on diverse properties.

In this contribution, we therefore compare the influence of different aryl flanking units as well as the influence of fluorination of the comonomer on the charge carrier mobility, optical properties, and crystallinity. The systematic variation of the structural units allows us to elucidate the influence of dihedral angles suggested in literature on moving from (a) thiophene over pyridine to phenyl as the aryl flanking unit in PDPP and (b) thiophene to difluoro-thiophene as comonomer. This interactive study is very essential to understand the positive as well as negative influences on optical properties and crystallinity when structural design is planned with an aim to improve electron transport. For this purpose, we synthesized a set of six DPP copolymers varying their flanking units and degree of fluorination in the comonomer. Two of these copolymers (herein denoted as PDPP$[T]_2$-T and PDPP$[Ph]_2$-T) having thiophene or phenyl flanking units along with thiophene as a comonomer are known in literature as PDPP3T[3a,4a] and PB,[17] respectively. To enable a comprehensive comparison of the newly synthesized systems with these known polymers, all the six copolymers were prepared using Stille polycondensation under similar synthetic conditions. This helps the evaluation of all the studied copolymers under the same conditions of measurement and device geometry in order to elucidate a structure–property relationship. The influence of structural variation on crystallinity was studied using Flash-DSC (dynamic scanning calorimetry), XRD

(X-ray diffraction), and polarization microscopy. In order to differentiate between any possible orientation effects as well as the influence of crystallinity on charge carrier mobility, all materials are measured under similar conditions, both in OFET and diode configuration (SCLC). Additionally, the influence of fluorination of the comonomer on charge carrier mobility is examined. This systematic and fundamental comparison gives valuable information for the further design of both donor and acceptor-type PDPP materials to suit the necessity of application.

Thus, in the design of electron transport DPP copolymers, we make use of two synthetic strategies based on the effects mentioned above: a) less steric hindrance between the DPP core and flanking aryl units by selecting a pyridyl group and b) perfluorinated thiophene as a comonomer. In this way a synergetic effect caused by both flanking units and comonomer may be expected and the resulting properties can be explained in terms of structural changes.

2. Results and Discussion

2.1. Nomenclature

Different approaches for naming diketopyrrolopyrrole derivatives are used in literature. Most of them are based on a non-systematic use of alphabets leading to an arbitrary name, which does not help to understand the chemical structure from the name. Therefore, we suggest to use a modular acronym approach (see Scheme 1) in this paper as per the following guidelines. The thiophene-DPP structures are shown in a conformation in accordance with the crystal structures of model compounds, in which the CO···HC interactions arising from the DPP and the flanking thiophene units seem predominating over the S–O interactions. In this nomenclature one can determine the molecular structure of the compound directly from the acronym without any additional aids.

Low molecular weight diketopyrrolopyrrole derivatives consist of a) the bicyclic DPP core, b) flanking aromatic units (**Ar**) adjacent to the core, c) solubilizing groups/side chains (R), and eventually d) terminal functional groups (**FG**). When comparing a series with identical side chains or when the side chains are negligible for discussion, the side chain may be omitted from the acronym for clarity. The flanking aryl units are put in square brackets as [**Ar**] followed by **FG**. For polymers, the comonomer $\mathbf{M_{co}}$ is given instead of the **FG** and delimited by a dash. For example, the dibromo-DPP monomer containing thiophene as flanking aromatic units can be represented as DPP[T]$_2$Br$_2$ and its copolymer using thiophene or phenyl as a comonomer as PDPP[T]$_2$-T and PDPP[T]$_2$-Ph, respectively. These two represent the polymers hitherto known in literature as PDPP3T[4a] and PDPPTPT.[1c,2]

2.2. Synthesis

The dibrominated thienyl-DPP **DPP[T]$_2$Br$_2$**,[18] pyridinyl-DPP **DPP[Py]$_2$Br$_2$**,[19] and phenyl-DPP **DPP[Ph]$_2$Br$_2$**[20] monomers were synthesized following modified literature procedures. 2,5-Bis(trimethylstannyl)-3,4-difluorothiophene was synthesized according to literature protocols.[21] Detailed procedures are given in the Supporting Information. For the synthesis of the nonfluorinated polymers, the dibromo-DPPs were coupled with the distannylthiophene. However, for the fluorinated polymers, it should be noted that bromo-functionalization of the electron-deficient difluoro-thiophene unit and stannyl-functionalization of the relatively more electron-rich DPP unit would be preferable for Stille-polycondensation.[22] But in terms of monomer purification, 2,5-dibromo-3,4-difluorothiophene as a liquid compound is difficult to purify on a small scale to an extend that is necessary for polycondensation. On the other hand, 2,5-bis(trimethylstannyl)-3,4-difluorothiophene can be obtained in high purity via recrystallization. Therefore we found it much more practical to use the functionalization in the reverse order as shown in Scheme 1. In order to obtain high degrees of polymerization, the purity and stoichiometry of the monomers in polycondensation is highly relevant. Polymerizations were carried out in chlorobenzene at 180 °C under microwave conditions in pressurized and sealed vials.[23] All polymers were endcapped with thiophene on both ends.

2.3. Characterization

2.3.1. Gel Permeation Chromatography (GPC)

The polymers were obtained with number average molecular weights (M_n) in the range of 10 700–40 800 g mol^{-1} and polydispersities ($Đ$) between 1.6 and 4.0 (**Table 1**) in good yields. GPC traces (Supporting Information Figures S1–S6) show a monomodal distribution for all polymers except PDPP[T]$_2$-TF$_2$, which exhibits a shoulder. The GPC traces of PDPP[T]$_2$-T and

Table 1. GPC and thermal data of the synthesized PDPPs.

Polymer	M_n[a] [kg mol^{-1}]	M_w[a] [kg mol^{-1}]	M_p[a] [kg mol^{-1}]	$Đ$[b]	DP$_n$[c]	Yield	T_m[d] [°C]
PDPP[T]$_2$-T	34.2	107.7	81.7	3.1	41	79%	290
PDPP[T]$_2$-TF$_2$	40.8	161.9	137.0	4.0	47	81%	331
PDPP[Py]$_2$-T	19.6	54.0	37.4	2.8	24	74%	294
PDPP[Py]$_2$-TF$_2$	12.0	29.2	24.2	2.3	14	69%	333
PDPP[Ph]$_2$-T	10.7	25.3	21.5	2.4	13	87%	–
PDPP[Ph]$_2$-TF$_2$	14.4	22.8	16.4	1.6	17	58%	–

[a]Determined by GPC at 150 °C using 1,2,4-trichlorobenzene as the eluent; [b]Polydispersity; [c]DP calculated from M_n; [d]Melting peak values from Flash-DSC.

PDPP[T]$_2$-TF$_2$ exhibit very high peak molecular weights in the range of 10^5 g mol^{-1} unlike the others having peak molecular weights (M_p) less than 40 kg mol^{-1}. Since all polymerizations were carried out under comparable conditions of temperature, time, monomer purity, and concentration, the very high molecular weight values might be attributed to aggregation of the highly crystalline thienyl-derivatives under the GPC measurement conditions. Accordingly, the number average degree of polymerization (DP$_n$) shows differences for the distinct PDPPs. The PDPP[T]$_2$ polymers were obtained with a DP$_n$ of 41 and 47 whereas the PDPP[Py]$_2$ and PDPP[Ph]$_2$ polymers show a DP$_n$ of 13–24. The flanking aryl units on the DPP core also have a severe effect on solubility. The PDPP[T]$_2$ polymers are only soluble in chloroform at room temperature and *o*-dichlorobenzene or 1,2,4-trichlorobenzene at elevated temperatures. PDPP[Py]$_2$ and PDPP[Ph]$_2$ polymers are much more soluble (e.g., in hexane or THF). It should be noted that the fluorinated polymer PDPP[Py]$_2$-TF$_2$ is insoluble in hexane although its molecular weight is considerably smaller than that of the nonfluorinated reference polymer PDPP[Py]$_2$-T, which is soluble in hexane. This is attributed to a rigidification of the backbone and hence a higher tendency for aggregation for the fluorinated derivatives.

2.3.2. Thermal Properties

In general, PDPPs exhibit very high melting points almost near their respective degradation temperatures depending on the backbone rigidity and nature of the alkyl chains. Therefore we adopted Flash-DSC measurements to avoid any degradation and to obtain comparative transition temperatures with a single method. Melting points of the PDPPs as measured on a Flash-DSC with heating rates from 50 to 1000 K s^{-1} are summarized in Table 1. All the DSC curves can be found in Supporting Information Figure S7. With regard to the flanking aryl units, the PDPP[T]$_2$ and PDPP[Py]$_2$ systems exhibit a melting point in Flash-DSC measurements. Further, the fluorination via comonomer increases the melting point drastically by about 40 °C. Thus, the nonfluorinated polymers PDPP[T]$_2$-T and PDPP[Py]$_2$-T show a similar melting point of 290 °C, whereas the fluorinated derivatives PDPP[T]$_2$-TF$_2$ and PDPP[Py]$_2$-TF$_2$ have melting points of 331 and 333 °C, respectively. Both of the PDPP[Ph]$_2$ polymers show neither a melting point nor a glass transition temperature in the DSC curves up to 400 °C, which indicates negligible crystallinity. To further explore the presence of any low-enthalpic transition, such as liquid-crystalline clearing which can be overseen in a flash-DSC measurement, PDPP[Ph]$_2$-T and PDPP[Ph]$_2$-TF$_2$ were examined using a polarization microscope. The polarization micrographs are given in Supporting Information Figure S8. It is evident that both of these polymers show liquid crystalline behavior in the range of 140–270 °C. Under crossed polarizers the shearable, birefringent textures observed in this range disappear on clearing, which can be reversibly observed on cooling.

2.3.3. Optical Properties

The optical absorption and photoluminescence (PL) spectra of all the polymers in solid state are shown in **Figure 1**. Additional spectra in solution can be found in Supporting Information Figure S9. For all comparable pairs (fluorinated vs nonfluorinated), the absorption onsets in solid state compared to those in solution exhibit a redshift of about 50 nm due to aggregation as expected for these semicrystalline polymers (Figure 1a); the smallest shift being observed for the less-ordered PDPP[Ph]$_2$ system. The flanking aryl units show pronounced influence on both spectral nature and onset. Thus, the spectral signatures change drastically from PDPP[Ph]$_2$-T to PDPP[T]$_2$-T; the broad structureless spectra transform to well-structured spectra having vibronic bands. This indicates that the aggregation due to crystallization increases from phenyl- to thienyl-flanked

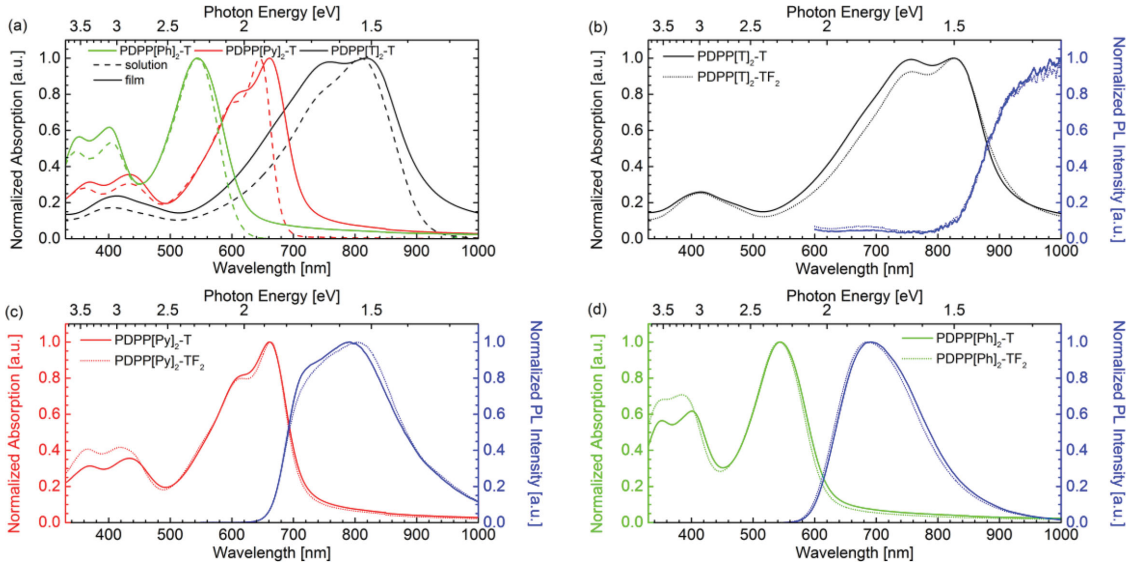

Figure 1. Absorption and PL spectra comparing the influence of a) the flanking aryl unit in film and solution for the nonfluorinated copolymers and b–d) fluorination of the comonomer in solid state for each pair. For solution spectra see Supporting Information Figure S9.

DPPs. The optical gaps were calculated from the absorption onset in thin film via tangential fitting. Thus, the flanking aryl unit next to the DPP core shows a considerable influence on the absorption onset as well. The optical gaps for PDPP[T]$_2$-T, PDPP[Py]$_2$T, and PDPP[Ph]$_2$-T are 1.3, 1.7, and 2.0 eV, respectively (Figure 1). The fluorination of the comonomer in all the three types of copolymers does not have any considerable influence either on spectral nature or on absorption onset in thin films (see Figure 1b–d). However, there are small changes in the absorption peak in solution spectra (Supporting Information Figure S9) for some of the fluorinated derivatives. For example, PDPP[T]$_2$-T in solution peaks at 821 nm whereas the peak of PDPP[T]$_2$-TF$_2$ is 15 nm redshifted to 836 nm. Similarly, for the PDPP[Ph]$_2$ derivatives also a redshift in absorption occurs only in solution. In the PDPP[Py]$_2$ system the absorption is not redshifting upon fluorination.

The PL intensity for phenyl- is larger than for pyridyl-substituted PDPPs, whereas the thiophene-derivatives exhibit only negligible PL. Both the PDPP[T]$_2$ polymers exhibiting the smallest optical gaps with absorption in the NIR range show PL beyond our detection limit of 1000 nm. Generally speaking, fluorination seems to have only little effect on the PL of the investigated polymers as is the case for absorption.

The change in absorption onset upon variation of the flanking aryl unit can be explained with the help of planarization/delocalization effects. To give a quantitative assessment, we make use of published single crystal data available in the CCDC (Cambridge Crystallographic Data Centre) library. When discussing the backbone planarity of these three systems, PDPP[T]$_2$-**M$_{co}$**, PDPP[Py]$_2$-**M$_{co}$**, PDPP[Ph]$_2$-**M$_{co}$**, experimental crystal structures from the corresponding low molecular weight diaryl-DPP compounds are used in the following. For the well-known DPP[T]$_2$ system several crystal structures are published. The dihedral angle α is ranging from 3° to 9° (see Supporting Information Table S1). The phenyl-DPP motif shows drastically larger dihedral angles of 26°–28°. For pyridinyl-DPP no applicable reference systems are available and therefore no estimation regarding the dihedral angle in our DPP[Py]$_2$ system can be made.

Regarding the dihedral angle β only few crystal structures with the motifs used in this study are published. Accordingly, the β-values could be comparatively estimated only for the polymers PDPP[T]$_2$-T and PDPP[T]$_2$-TF$_2$. Thus, angles in nonfluorinated oligothiophene (2°–6°, see Supporting Information Table S2) are only slightly larger than angles in perfluorinated oligothiophenes (0°–3°). Crystal structures of pyridine or phenyl rings adjacent to 3,4-difluorothiophene are not published to the best of our knowledge. Based on crystallinity data, it can be concluded that the phenyl flanking units lead to a considerable backbone twist which is not present in the thiophene system. For the 2-pyridyl system, which lacks the H-atom at 2-position no steric hindrance and, therefore, no considerable backbone twist is expected.

2.3.4. Cyclic Voltammetry

The electrochemical behavior of all the polymers was studied with respect to reversibility as well as redox potentials. The individual cyclic voltammograms are given in Supporting Information Figure S10 and the comparison of the energy levels is shown in **Figure 2**. The energy levels of the PDPPs were calculated from the redox potentials calibrated against ferrocene using a published procedure taking into account solvent effects.[24] All the redox-potential values were obtained by cyclic voltammetry on polymer thin films with indium tin oxide (ITO) as the working electrode. For values obtained from cyclic voltammetry, Bredas has recommended to use ionization potential (IP) and electron affinity (EA) rather than HOMO and LUMO, respectively.[25] All the six polymers show typical reversible oxidation and reduction waves as known for other PDPPs in literature.[26] The variation of the flanking aryl units from thiophene to pyridyl and phenyl shifts both IP and EA resulting in the broadest electrochemical gap E_{CV} for the PDPP[Ph]$_2$ polymers. The smallest electrochemical gap observed for PDPP[T]$_2$-T is similar to the observations in the optical gap measurements discussed above.

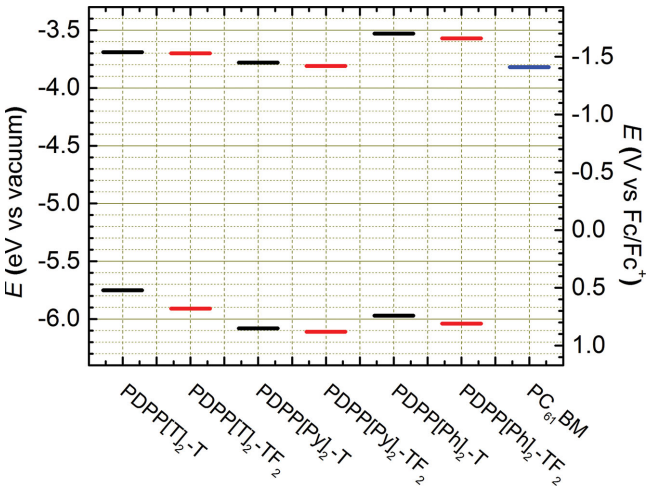

Figure 2. Energy level comparison for the synthesized polymers determined by cyclic voltammetry in thin film. The solid state reduction potential of PC$_{71}$BM (−1.41 eV) corresponding to an EA of −3.82 eV is shown for comparison.

The effect of fluorination is pronounced on the oxidation potential of PDPP[T]$_2$-TF$_2$. Otherwise, the influence is almost negligible on both IP and EA for the other derivatives. For example, the IP is increased from 5.75 eV for PDPP[T]$_2$-T by 0.16–5.91 eV for PDPP[T]$_2$-TF$_2$. On the other hand the EA is not affected by fluorination giving a value of 3.70 eV for both PDPP[T]$_2$-T and PDPP[T]$_2$-TF$_2$. Thus, the electrochemical gap increases in the PDPP[T]$_2$ system whereas no influence is observed for the PDPP[Py]$_2$ and PDPP[Ph]$_2$ systems upon fluorination. Comparing the differently flanked DPP units the PDPP[T]$_2$ polymers show the smallest, whereas the PDPP[Ph]$_2$ polymers show the highest electrochemical gap, which is in accordance with previous considerations on the degree of delocalization and the strength of the inherent D–A–D push/pull systems. The EA value for PDPP[Py]$_2$-TF$_2$ is −3.81 eV and it is comparable to the EA of the commonly used acceptor PC$_{71}$BM (Figure 2).

The difference in optical and electrochemical gap [$\Delta(E_{opt} - E_{CV}$] varies considerably from the PDPP[T]$_2$ over

Table 2. Solid state electrochemical and structural properties of the PDPPs.

Polymer		Cyclic voltammetry				XRD			
	IP[a] [eV]	EA[b] [eV]	E_{cv}[c] [eV]	E_{opt}[d] [eV]	d_{lam}[e] [Å]	d_{amorph}[f] [Å]	$d_{\pi-\pi}$ [Å]	z[g] [nm]	ζ_{lam}[h]
PDPP[T]$_2$-T	−5.75	−3.69	2.06	1.32	19.16	4.52	3.86	6.9	
PDPP[T]2-TF2	−5.91	−3.70	2.21	1.33	19.83	4.40	3.65	8.8	
PDPP[Py]$_2$-T	−6.08	−3.78	2.30	1.72	19.05	4.56	3.91	3.9	
PDPP[Py]$_2$-TF$_2$	−6.11	−3.81	2.30	1.73	18.63	4.48	3.90	4.1	
PDPP[Ph]$_2$-T	−5.97	−3.53	2.44	1.98	14.94	–	4.04		2.7
PDPP[Ph]$_2$-TF$_2$	−6.04	−3.57	2.47	2.03	14.62	–	3.90		2.1

[a]CV based ionization potential; [b]CV based EA; [c]Electrochemical gap determined by CV in thin film; [d]Optical gap determined from absorption onset in film; [e]Lamellar spacing; [f]amorphous peak; [g]$\pi-\pi$ spacing; [h]Crystal correlation length $\zeta = 2\pi/\text{FWHM}$ of the lamellar spacing.

PDPP[Py]$_2$ to PDPP[Ph]$_2$ polymers (**Table 2**). The influence of fluorination is again pronounced only in the PDPP[T]$_2$ system. Thus, the highest $\Delta(E_{opt} - E_{CV})$ which gives a rough orientation for electron–hole pair binding energy is observed for PDPP[T]$_2$-TF$_2$ (0.88 eV) whereas the lowest value of 0.44 eV is obtained for PDPP[Ph]$_2$-TF$_2$.

2.3.5. Solid State Structure

Comparative crystallinity and lamellar spacing was estimated from transmission powder XRD measurements in the small and wide angle X-ray scattering (SAXS/WAXS) region (q = 0.016–2.86 Å^{-1}) of free standing bulk samples without any thermal treatment. The sharp peaks with small full width at half maximum (FWHM) values reach a correlation length up to 8.8 nm and are centered at $q \approx 0.3$ Å^{-1} indicating the lamellar spacing d_{lam}, whereas the broad peaks in the WAXS region represent the $\pi-\pi$ distances $d_{\pi-\pi}$ and amorphous polymer.[27] An overview of the periodic distances d_{lam} and $d_{\pi-\pi}$ as well as the correlation lengths ζ are given in Table 2 and the individual diffractograms are shown in **Figure 3**. Qualitatively, the intensity of the d_{lam} peaks is higher for the fluorinated polymers for all the three DPP derivatives (comparing normalized intensities) suggesting a higher crystallinity. On comparison of the influence of flanking aryl units, the PDPP[T]$_2$ polymers show the highest degree of crystallinity followed by the PDPP[Py]$_2$ polymers (Figure 3a). The PDPP[Ph]$_2$ polymers give the weakest d_{lam} signals showing only a small difference between nonfluorinated and fluorinated derivative. This is in accordance with the observations from DSC measurements. In general, the diffraction peaks at $q \approx 0.3$ Å^{-1}, corresponding to a inter-lamellar distance of around 19 Å, are hardly influenced by fluorination. The second order can be found for the PDPP[T]$_2$ and for the PDPP[Py]$_2$ polymers, indicating a good lamellar organization. On the other hand, the $\pi-\pi$ stacking distances decrease upon fluorination of the thiophene comonomer by about 0.1 Å suggesting a stronger $\pi-\pi$ interaction for the fluorinated derivatives. Furthermore, in the thienyl- and pyridinyl-DPP polymers the FWHM of the lamellar stacking peak is smaller for the fluorinated derivatives, which is indicating longer coherence length which may suggest larger crystals. This is also in agreement with the observed increase in melting points for those fluorinated derivatives.

2.4. Charge Transport Properties

In order to obtain a comprehensive picture regarding the influence of structural variation on charge carrier transport, we

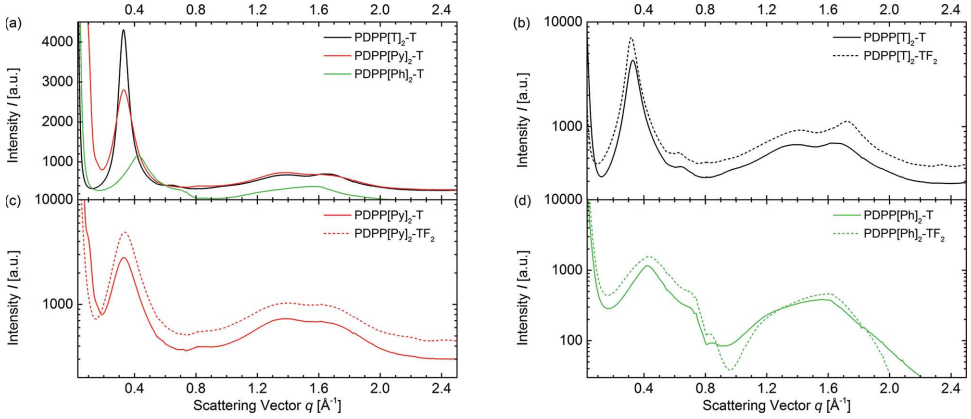

Figure 3. Bulk SAXS/WAXS measurements of the PDPPs: a) comparison of different flanking units and b–d) comparison of fluorinated with nonfluorinated derivatives.

Table 3. Average OFET-mobilities of the different PDPPs in a BGBC configuration in as cast and annealed films.

	As cast		Annealed[a)]	
Polymer	μ_h[b)] [cm^2 V^{-1} s^{-1}]	μ_e[b)] [cm^2 V^{-1} s^{-1}]	μ_h[b)] [cm^2 V^{-1} s^{-1}]	μ_e[b)] [cm^2 V^{-1} s^{-1}]
PDPP[T]$_2$-T	0.094 ± 0.02	–	0.53 ± 0.07[c)]	–
PDPP[T]$_2$-TF$_2$	0.10 ± 0.02	0.06 ± 0.01	0.22 ± 0.03[d)]	0.19 ± 0.03[d)]
PDPP[Py]$_2$-T	–	0.03 ± 0.003	–	0.55 ± 0.08[c)]
PDPP[Py]$_2$-TF$_2$	–	0.11 ± 0.02	–	0.13 ± 0.02[c)]
PDPP[Ph]$_2$-T	(6 ± 3) × 10^{-4}	–	(6 ± 2) × 10^{-4}[e)]	–
PDPP[Ph]$_2$-TF$_2$	(9 ± 0.4) × 10^{-5}	(2 ± 0.2) × 10^{-4}	(1 ± 0.5) × 10^{-4}[e)]	(2 ± 0.3) × 10^{-4} [e)]

[a)]Annealing conditions as described in footnote; [b)]μ_h: hole mobility, μ_e: electron mobility, determined by linear fitting of $I_{ds}^{0.5}$-plot in saturated regime, values are averaged over a minimum of four to eight devices for each measurement; [c)]250 °C, 30 min; [d)]200 °C, 15 min; [e)]100 °C, 15 min.

measured both OFET and SCLC mobilities for all the copolymers under as-cast as well as annealed conditions. In general, the charge carrier density in field effect transistors is higher than in the diode configuration and correspondingly the mean mobility is lower in SCLC measurements.[7] The former are also influenced by orientation effects at the semiconductor–dielectric interface whereas in the latter information regarding isotropic bulk charge carrier mobilities irrespective of interfacial orientation effects is obtained.

2.4.1. OFET

The OFET mobilities were obtained in thin films using a bottom gate/bottom contact (BGBC) configuration and are summarized in **Table 3**. For each data point, a minimum of four devices was measured. As a typical example, transfer and output curves of PDPP[T]$_2$-T and PDPP[T]$_2$-TF$_2$ are shown in **Figure 4**. The curves of the PDPP[Py]$_2$ and PDPP[Ph]$_2$ polymers are given in Supporting Information Figure S11. All devices exhibit very high on/off ratios ($I_{on/off}$: 10^5–10^8) unless operated at very high drain voltages. In this case (V_d = 80 V), the on/off ratio decreases to about 10^2 due to the ambipolar nature of the material. Detailed influence of the drain voltage on transfer characteristics is shown in Supporting Information Figure S12. All on/off ratios for different modes of operation are also given in Supporting Information Table S3. Most of the samples were either p-type or n-type in the as-cast films. Only PDPP[T]$_2$-TF$_2$ exhibits ambipolar characteristics with high mobility values (μ_h = μ_e = 0.2 cm^2 V^{-1} s^{-1}). Among the whole series, the PDPP[T]$_2$ system shows three orders of magnitude higher hole mobilities (μ_h = 10^{-1} cm^2 V^{-1} s^{-1}) than PDPP[Ph]$_2$ copolymers, which show the lowest values (μ_h = 10^{-4} cm^2 V^{-1} s^{-1}). In the case of pyridyl-flanked PDPPs no hole mobility could be measured even at high gate voltages. However, the highest electron mobility was observed for PDPP[Py]$_2$-TF$_2$ (μ_e = 10^{-1} cm^2 V^{-1} s^{-1}). Thus, the flanking aryl units have a very pronounced influence on the type of charge carrier transport, as well as charge carrier mobility values; thienyl being highly suitable for hole transport, whereas pyridyl for electron transport. In all the

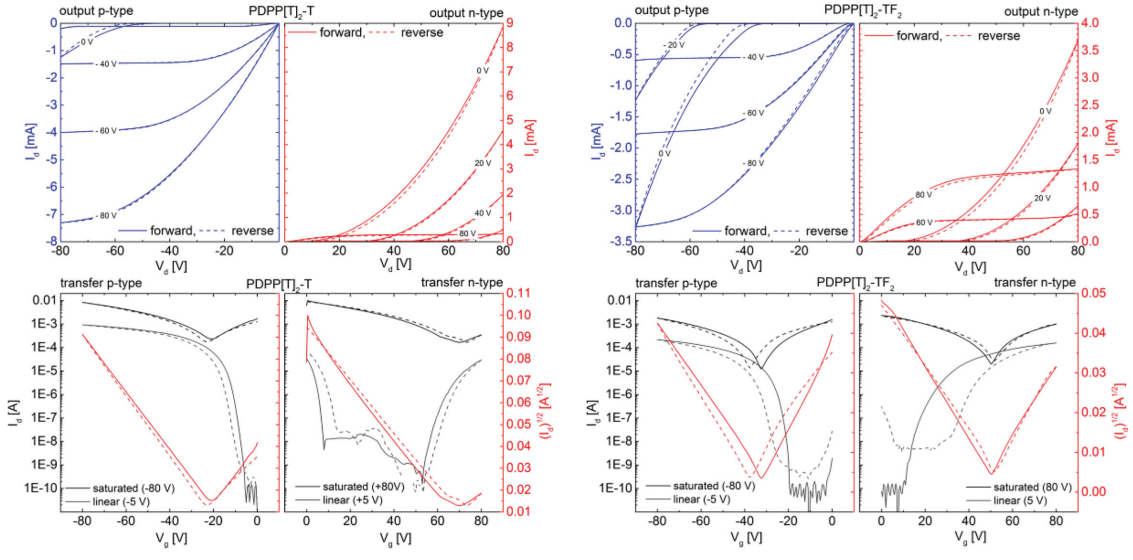

Figure 4. Representative OFET *I–V* curves in p-channel (blue output) and n-channel operation (red output) for PDPP[T]$_2$-T (left) and PDPP[T]$_2$-TF$_2$ (right). Solid lines represent forward scans, dashed lines the reverse scans in all graphs. In transfer curves (bottom), the black and gray plots indicate the transfer characteristics in the saturation and linear operation regime, respectively. *I–V* curves for the PDPP[Py]$_2$ and PDPP[Ph]$_2$ polymers can be found in Supporting Information Figure S12.

copolymers the fluorination of the comonomer improves the electron transport considerably in as cast films. In addition, a threshold voltage shift towards more negative voltages was observed for the fluorinated derivatives. Generally, all devices showed increased charge carrier mobilities upon thermal annealing. In order to exploit the improved crystalline packing during annealing, all the samples were annealed at the highest possible temperatures in the range of 200–250 °C, if the samples were not dewetting or showing decreased performance in this range. In the case of PDPP[Ph]$_2$ copolymers 100 °C was chosen due to dewetting issues in the liquid crystalline phase above this temperature. After annealing, the observed influence of the flanking aryl units remains. Additionally, the crystalline PDPP[T]$_2$ and PDPP[Py]$_2$ copolymers exhibit maximum influence of annealing on both hole and electron mobilities. Thus, the highest hole mobility was obtained for PDPP[T]$_2$-T (average: 0.53 cm^2 V^{-1} s^{-1}, best: 0.64 cm^2 V^{-1} s^{-1}) and the highest electron mobility for PDPP[Py]$_2$-T (average: 0.55 cm^2 V^{-1} s^{-1}, best: 0.67 cm^2 V^{-1} s^{-1}). These are very high charge carrier mobility values obtained for PDPPs using SiO_2 as the gate dielectric. For example, a one order of magnitude lower hole mobility (0.05 cm^2 V^{-1} s^{-1}) was reported for the reference copolymer PDPP[T]$_2$-T.[4a] The liquid crystalline PDPP[Ph]$_2$ copolymers do not exhibit any change in either hole or electron mobility on thermal treatment. The observed charge carrier properties can be summarized as follows: The highly crystalline copolymers exhibit the highest charge carrier mobilities whereas the liquid crystalline copolymers show three orders of magnitude lower values. On annealing, the mobility is improved only for the crystalline samples. With respect to flanking aryl units, both thiophene and pyridyl with the smallest dihedral angles favor high mobilities which can be understood as due to improved planarization and interchain packing. Additionally, no detectable hole mobility and the highest electron mobility in the whole series was observed for the pyridyl-flanked PDPPs. The effect of fluorination is also pronounced in the electron mobility values. The exact contribution of orientation effects in these samples, especially in the crystalline ones, cannot be elucidated without additional experimental techniques, such as near edge X-ray absorption fine-structure spectroscopy (NEXAFS) or grazing incidence wide angle X-ray scattering (GIWAXS).

2.4.2. SCLC

To study the influence of electron-rich and electron-deficient moieties as aryl-flanking units and comonomers on bulk charge transport properties, both hole and electron mobilities were determined by fitting measured *I–V* characteristics using the empirical Murgatroyd formula (Equation (1)[28] in single carrier SCLC devices.

$$J = \frac{9}{8}\varepsilon_s\varepsilon_0\mu_0 \exp(0.89\gamma\sqrt{F})\frac{V^2}{L^3} \quad (1)$$

Here J is the current density, ε_s is the relative permittivity of the material (≈3.5), ε_0 is the permittivity of vacuum, μ_0 is the charge carrier mobility at zero field, γ is the field dependence parameter, F is the average electric field across the active layer, V is the voltage across the active layer, and L is the thickness of the polymer layer. In the Murgatroyd formula two independent variables, namely the zero field mobility (μ_0) and the field dependence parameter (γ), are varied to fit the measured *I–V* curve. The usefulness of the Murgatroyd formula over the classical Mott–Gurney equation[29] is that it is able to fit a broader range of *I–V* curves and also masks other effects, such as charge carrier-density dependent transport[30] and trapping influence.[31] However, γ is generally very sensitive to disorder and to the electrodes of the device. It is therefore hard to determine in a consistent way for different devices.[32] To compare the bulk charge transport properties of a series of materials in a simple and consistent way, an effective charge carrier mobility was determined from all devices at a same field, $F = 1.5 \times 10^7$ V m^{-1}, using the Poole–Frenkel relationship (Equation (2)):

$$\mu(F) = \mu_0 \exp(\gamma\sqrt{F}) \quad (2)$$

The reporting of charge mobility at a constant field summarizes the information of two independent parameters (μ_0 and γ) in a single parameter and allows a straightforward charge mobility comparison across different materials.[33] The field value, $F = 1.5 \times 10^7$ V m^{-1}, was chosen as it represents a typical field at short circuit condition in thin film solar cell devices and also the SCLC fits were good around this field value for all the *I–V* curves reported in this article.

The charge mobility value in every as-cast film was checked for reproducibility and consistency by repeating the experiment for different active layer thicknesses (Supporting Information Figure S13). Representative *I–V* curves of different PDDPs for as-cast films in hole-only and electron-only devices are shown in **Figure 5**a,b, respectively. The effective hole and electron mobilities averaged over different film thickness devices are depicted in Figure 5c,d. **Table 4** summarizes the charge carrier mobilities of holes and electrons in PDPP films averaged over different thicknesses. A complete table listing film thicknesses and fitting parameters for all the devices can be found in Supporting Information Tables S4 and S5. Furthermore, the charge carrier mobilities from the annealed films are also depicted in Figure 5c,d and the mobility values are mentioned in Table 4. As shown in Figure 5c, the SCLC hole mobility does not vary significantly for the investigated set of materials. The hole mobility in all cases was in the order of 10^{-5} cm^2 V^{-1} s^{-1} and seemed not to be affected by fluorination either. It is interesting to note that the hole mobility measured in OFETs was in the order of 10^{-1} cm^2 V^{-1} s^{-1} for all polymers except the PDPP[Ph]$_2$ system. In contrast to the hole transport, the electron mobility was severly influenced by the aryl flanking unit. Both PDPP[T]$_2$-T and PDPP[T]$_2$-TF$_2$ showed the lowest bulk electron mobilities in the order of 10^{-8} cm^2 V^{-1} s^{-1}. In comparison, the PDPP[Py]$_2$-T shows up to 4 orders of magnitude better electron mobility ($\mu_e = 3.7 \times 10^{-4}$ cm^2 V^{-1} s^{-1}). The electron transport in the PDPP[Ph]$_2$ polymers was in between thienyl- and pyridinyl-PDPPs with mobilities in the range of $\mu_e = 3 \times 10^{-5}$ cm^2 V^{-1} s^{-1}. Upon fluorination, PDPP[Py]$_2$-TF$_2$, exhibits a considerable improvement of an order of magnitude in electron mobility resulting in a maximum bulk electron mobility of 4.3×10^{-3} cm^2 V^{-1} s^{-1}. To the best of our knowledge, this is among the highest bulk electron mobilities reported for

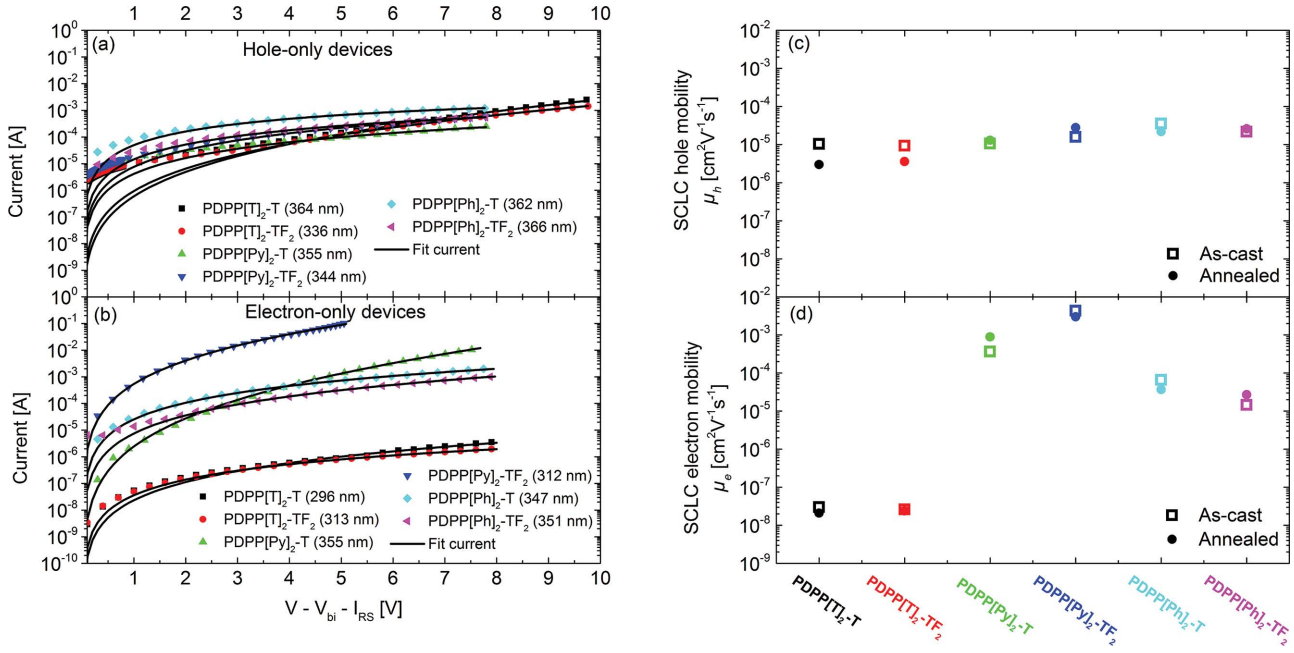

Figure 5. The *I–V* characteristics of as-cast PDDP films measured at room temperature in a) hole-only and b) electron-only device configuration. The solid lines represent the SCLC fit with field dependent mobility. The corresponding film thicknesses are mentioned within the parentheses. The *I–V* characteristics were corrected for the built-in voltage (V_{bi}) and the voltage drop (IR) over the contacts. Log–log plots of (a,b) are given in Supporting Information Figure S14. The effective SCLC charge carrier mobility of c) holes and d) electrons at an electric field of 1.5×10^7 V m^{-1} in different PDDP films. The mobility in as-cast films is depicted as unfilled squares while that in annealed films as filled circles. Each as-cast data point represents the average of three sets of devices produced for varying film thicknesses in the range of 200–600 nm.

polymers[34] and it is comparable to electron mobilities reported for fullerene derivatives.[35] Annealing does not seem to influence either of the hole or electron mobility values suggesting that the expected crystallization effects in annealed films do not overcome grain-boundary effects in a bulk sample which do not have any orientation preferences. This is in contrast to the observed advantages of annealing in an interface-device, such as OFET, where orientation effects can play a big role. In short, the electron mobility results demonstrate that the flanking aromatic units (**Ar**) adjacent to the bicyclic DPP core have a more significant influence on the bulk electron transport than the fluorination in the class of PDPP. Moreover, the synthetic strategy to combine a pyridyl-flanking unit with a difluorothiophene comonomer proved to be highly efficient for electron transport.

3. Conclusion

Six polymers based on diketopyrrolo[3,4-*c*]pyrrole having varying flanking aryl units and thiophene or 3,4-difluorothiophene as the comonomer have been synthesized in order to elucidate the influence of structural variation on optical, thermal and electronic properties. This is the first comprehensive and comparative study of interdependence of diverse properties obtained via a change in chemical structure. On a comparison of flanking units, namely thiophene, pyridine and phenyl, profound influence on structural order, optical gap and charge carrier properties could be ascertained. For example, thienyl or pyridyl flanking units causing low dihedral angles favor planarization of the chains and interchain packing in solid state resulting in low optical gap, high structural order and very high charge

Table 4. The average effective SCLC charge carrier mobility of holes (μ_h) and electrons (μ_e) in PDPP as-cast films for varying film thicknesses. The charge mobility in annealed films for single film thickness (around 350 nm) is also mentioned. The thienyl- and pyridinyl-films were annealed at 200 °C for 15 min. The phenyl-films were annealed at 100 °C for 15 min.

	As cast		Annealed	
Polymer	μ_h [cm^2 V^{-1} s^{-1}]	μ_e [cm^2 V^{-1} s^{-1}]	μ_h [cm^2 V^{-1} s^{-1}]	μ_e [cm^2 V^{-1} s^{-1}]
PDPP[T]$_2$-T	$(1.0 \pm 0.5) \times 10^{-5}$	$(3.0 \pm 0.9) \times 10^{-8}$	3.0×10^{-6}	2.1×10^{-8}
PDPP[T]$_2$-TF$_2$	$(9.4 \pm 3.3) \times 10^{-6}$	$(2.6 \pm 1.5) \times 10^{-8}$	3.6×10^{-6}	2.4×10^{-8}
PDPP[Py]$_2$-T	$(1.1 \pm 0.9) \times 10^{-5}$	$(3.7 \pm 2.5) \times 10^{-4}$	1.3×10^{-5}	8.9×10^{-4}
PDPP[Py]$_2$-TF$_2$	$(1.6 \pm 0.7) \times 10^{-5}$	$(4.3 \pm 0.1) \times 10^{-3}$	2.8×10^{-5}	3.0×10^{-3}
PDPP[Ph]$_2$-T	$(3.6 \pm 0.2) \times 10^{-5}$	$(6.6 \pm 3.1) \times 10^{-5}$	2.2×10^{-5}	3.7×10^{-5}
PDPP[Ph]$_2$-TF$_2$	$(2.2 \pm 0.1) \times 10^{-5}$	$(1.5 \pm 0.6) \times 10^{-5}$	2.6×10^{-5}	2.7×10^{-5}

carrier mobilities. On the other hand, the phenyl flanking unit, which leads to large torsional angles in the polymer backbone, causes a 2D liquid crystalline order and also shows the lowest charge carrier mobilities. In addition to the flanking aryl units the physical properties could also be tuned by using suitable comonomers varying in their electron deficiency. Thus, 3,4-difluorothiophene comonomer in combination with the electron withdrawing pyridyl flanking unit delivers one of the best electron transport polymer materials with a comparable bulk electron mobility to PCBM ($\mu_e = 4 \times 10^{-3}$ cm^2 V^{-1} s^{-1}). An additional effect of fluorination is the increased crystallinity irrespective of the nature of flanking aryl units. This can be understood as due to decreased polymer chain-mobility in the fluorinated copolymers induced by a higher rigidity of the backbone and stronger π–π interactions. Such a detailed fundamental study regarding the influence of structural variation on semiconductor polymer properties allows a rational design of low-bandgap polymers in order to tune one or the other physical properties relevant for applications. Thus, the absorption can be extended up to the NIR region by shifting the absorption onset to >1000 nm by changing the flanking unit from phenyl to thiophene. On the other hand, the incorporation of pyridyl units without any steric hindrance with the DPP core maintains the crystallinity resulting in very good electron transport materials. A comparison of OFET and SCLC measurements gives a clear picture regarding the different contributions towards charge transport properties in thin film and bulk which are relevant for organic electronics and OPV applications. For example, the pyridinyl-flanked DPP copolymers show exclusively n-type behavior in OFET configuration whereas good ambipolar transport is observed in bulk SCLC measurements. Interestingly, the bulk hole mobility is completely independent of the nature of flanking units as well as fluorination of the comonomer. On the contrary, the electron transport is strongly influenced by these structural variations.

4. Experimental Section

Materials and Methods: All commercial reagents were used without further purification unless otherwise noted. Microwave reactions were conducted in sealed containers using a Biotage Initiator Eight+ microwave. ^{1}H NMR (300 MHz) spectra were recorded on a Bruker AC 300 spectrometer and calibrated according to the respective solvent resonance signal. GPC analysis was carried out on an Agilent (Polymer Laboratories Ltd.) PL-GPC 220 high temperature chromatographic unit equipped with DP (differential pressure), RI (refractive index), and LS (light scattering at 15° and 90°) detectors and three linear mixed bed columns of PLgel 13 µm (Olexis) with a linear MW operating range: 500–15 000 000 g mol^{-1}. GPC analysis was performed at 150 °C using 1,2,4-trichlorobenzene as the mobile phase. The samples were prepared by dissolving the polymer (0.1 wt%) in the mobile phase solvent in an external oven and the solutions were run without filtration. The molecular weights of the samples were referenced to linear polystyrene (M_w = 162–6 000 000 g mol^{-1}, K = 12.100, and Alpha = 0.707) and were not corrected with K and Alpha values for the measured sample. Cyclic voltammetry was performed under moisture- and oxygen-free conditions using a 0.1 M tetra-*n*-butylammonium hexafluorophosphate in acetonitrile electrolyte solution. A standard three-electrode assembly connected to a potentiostat (model 263A, EG&G Princeton Applied Research) was used at a scanning rate of 100 mV s^{-1}. The working electrode was a 10 Ω sq^{-1} ITO coated glass substrate. The polymers were spincoated onto the ITO substrates from chloroform at 3 mg mL^{-1} and 1500 rpm to obtain thicknesses of 10–20 nm. A platinum wire in acetonitrile was used as counter electrode and the quasi-reference electrode consisted of an Ag wire in an $AgNO_3$/acetonitrile solution (0.1 M). The measurements were calibrated with an external ferrocence/ferrocenium standard, IP and EA values were calculated considering the solvent effects as per a published procedure[24a] using Equations (3) and (4) where the workfunction of Fc/Fc$^+$ is taken to be −5.23 eV. The reduction half-step potential $E^{red}_{1/2}$(vsFc / Fc$^+$) is negative whereas the oxidation half-step potential $E^{ox}_{1/2}$(vsFc / Fc$^+$) is positive.

$$EA \approx -5.23 - E^{red}_{1/2}(\text{vs Fc} / Fc^+) \quad (3)$$

$$IP \approx -5.23\text{eV} - E^{ox}_{1/2}(\text{vs Fc} / Fc^+) \quad (4)$$

Absorption measurements were carried out on a JASCO V-670 spectrophotometer. PL measurements were carried out on a JASCO FP-8600 spectrofluorometer. Optical properties in solution were measured in chloroform at a concentration of 0.01 mg mL^{-1}, films were spincoated on glass slides from a 7 mg mL^{-1} chloroform solution. Combined SAXS and WAXS measurements of the bulk material were carried out at the SAXS beamline of the Australian Synchrotron using a Pilatus 1M and a Pilatus 200k detector. The beam energy and detector distances were chosen in such a way, that there was a small overlap between the SAXS and WAXS signal, so that the resulting curves could be stiched together at $q = 0.81$.

Device Preparation and Characterization: Organic thin film transistors substrates in BGBC configuration were bought from Fraunhofer IPMS (OFET Gen. 4). Heavily n-doped silicon (doping at wafer surface: $n \approx 3 \times 10^{17}$ cm^{-3}) was used as substrate and gate electrode. Thermally grown silicon oxide (230 ± 10 nm) was used as the gate dielectric. Gold electrodes (30 on 10 nm ITO as adhesion layer) were used as source and drain contacts. The channel width was 10 mm for all devices and the channel length varied from 5 to 20 µm. The substrates were cleaned subsequently in acetone and 2-propanol in an ultrasonic bath for 10 min each. Treatment in an ozone oven at 50 °C for 20 min was followed by immersion in a 1 wt% solution of octadecyltrichlorosilane in toluene at 60 °C for 60 min. After rinsing with toluene and 2-propanol the substrates were dried and the polymer was spincoated from a 4 mg mL^{-1} chloroform solution at 5000 rpm under ambient conditions. Devices were measured in a nitrogen atmosphere using an Agilent B1500 Semiconductor Parameter Analyzer. The devices were annealed in a nitrogen atmosphere at a maximum of 0.9 ppm O_2 at the temperatures given in the main text. Mobilities were calculated from the slopes in the $(I_d)^{0.5}$–V_g plots in the saturation regime using Equation (5) where I_d is the drain current, W is the channel width, L is the channel length, C_i is the capacitance, V_g is the gate voltage, and V_T is the threshold voltage, respectively.

$$I_d \approx \frac{W}{2L} C_i \mu (V_g - V_T)^2 \quad (5)$$

Single carrier space-charge-limited-current (SCLC) devices in diode configuration were prepared for charge carrier mobility determination of holes and electrons within the layer stack of glass/ITO/PEDOT:PSS/Polymer/Au and glass/ITO/PEDOT:PSS/Polymer/Ca/Al, respectively. For hole only devices, a hole-injecting layer of PEDOT:PSS (HTL solar (40 nm) from Clevios) was spin coated onto cleaned patterned ITO glass substrates. For electron-only devices, a 40 nm thick layer of Zinc oxide (ZnO) was spin coated onto the patterned substrates using Sol–gel method. After depositing the bottom layers, polymer solutions (12–25 mg mL^{-1} in chloroform) were doctor bladed on top under inert conditions resulting in film thicknesses in the range of 200–600 nm. A set of films were also annealed in an inert atmosphere for 15 min at the temperatures given in the main text. Subsequently, the top electrodes (Au and Ca/Al) were thermally evaporated onto the polymer layers in respective devices under high vacuum. The devices had an active area of 9 mm^2 which is determined by the overlap of the ITO and the evaporated top electrode. Dark current–voltage I–V measurements were

made under inert environment at room temperature with a Keithley 2400 source measure unit. Before these *I–V* measurements, the electron-only devices were exposed to 100 mW cm^{-2} illumination for 3 min from an AM 1.5 class A solar simulator to improve the conductivity of the ZnO layer.[36] After the light treatment, the *I–V* from the electron-only devices were nearly symmetric around 0 V. For mobility evaluation, forward bias voltages, that is, hole injection from PEDOT:PSS, and reverse bias voltages, i.e., electron injection from ZnO were considered in hole-only and electron-only devices, respectively. The charge carrier mobilities were evaluated by fitting measured *I–V* characteristics in a voltage range from 2 to 7 V using the Murgatroyd formula.[28] Prior to fitting, the measured *I–V* characteristics were corrected for the built in voltage (V_{bi}) and the voltage drop (IR) across contacts. The contact resistance was determined from a reference device without polymer layer and was found to be 27 Ω for both kind of devices. Considering the work function of the electrons and the Fermi-level pinning[37] at contacts, the V_{bi} of 0.2 and 0.0 V was assumed for hole-only and electron-only devices, respectively.

Supporting Information

Supporting Information is available from the Wiley Online Library or from the author.

Acknowledgements

We acknowledge financial support from DFG (SFB 840) and the Bavarian State Ministry of Education, Science and the Arts (Solar technologies go hybrid). C.J.M. thanks the Fonds der Chemischen Industrie for funding the PhD with a Kekulé scholarship and the German National Academic Foundation (Studienstiftung des deutschen Volkes) for additional support during the PhD. Support from the Elitenetzwerk Bayern (ENB Macromolecular Science), Macromolecular Science is also kindly acknowledged. Part of this research was undertaken on the SAXS/WAXS beamline at the Australian Synchrotron, Victoria, Australia.

Received: December 22, 2014
Revised: February 17, 2015
Published online: March 23, 2015

[1] a) S. Qu, H. Tian, *Chem. Commun.* **2012**, *48*, 3039; b) C. B. Nielsen, M. Turbiez, I. McCulloch, *Adv. Mater.* **2012**, *25*, 1859; c) J. C. Bijleveld, V. S. Gevaerts, D. Di Nuzzo, M. Turbiez, S. G. J. Mathijssen, D. M. de Leeuw, M. M. Wienk, R. A. J. Janssen, *Adv. Mater.* **2010**, *22*, E242; d) S. Holliday, J. E. Donaghey, I. McCulloch, *Chem. Mater.* **2014**, *26*, 647.

[2] W. Li, K. H. Hendriks, A. Furlan, W. S. Roelofs, S. C. Meskers, M. M. Wienk, R. A. Janssen, *Adv. Mater.* **2014**, *26*, 1565.

[3] a) J. C. Bijleveld, R. A. M. Verstrijden, M. M. Wienk, R. A. J. Janssen, *J. Mater. Chem.* **2011**, *21*, 9224; b) W. Li, K. H. Hendriks, A. Furlan, W. S. C. Roelofs, M. M. Wienk, R. A. J. Janssen, *J. Am. Chem. Soc.* **2013**, *135*, 18942; c) H. Bronstein, E. Collado-Fregoso, A. Hadipour, Y. W. Soon, Z. Huang, S. D. Dimitrov, R. S. Ashraf, B. P. Rand, S. E. Watkins, P. S. Tuladhar, I. Meager, J. R. Durrant, I. McCulloch, *Adv. Funct. Mater.* **2013**, *23*, 5647.

[4] a) J. C. Bijleveld, A. P. Zoombelt, S. G. J. Mathijssen, M. M. Wienk, M. Turbiez, D. M. de Leeuw, R. A. J. Janssen, *J. Am. Chem. Soc.* **2009**, *131*, 16616; b) S. Venkatesan, N. Adhikari, J. Chen, E. C. Ngo, A. Dubey, D. W. Galipeau, Q. Qiao, *Nanoscale* **2014**, *6*, 1011.

[5] S. Cho, J. Lee, M. Tong, J. H. Seo, C. Yang, *Adv. Funct. Mater.* **2011**, *21*, 1910.

[6] J. H. Park, E. H. Jung, J. W. Jung, W. H. Jo, *Adv. Mater.* **2013**, *25*, 2583.

[7] C. Tanase, E. J. Meijer, P. W. M. Blom, D. M. de Leeuw, *Phys. Rev. Lett.* **2003**, *91*, 216601.

[8] W. Li, W. S. Roelofs, M. Turbiez, M. M. Wienk, R. A. Janssen, *Adv. Mater.* **2014**, *26*, 3304.

[9] a) J. Lee, M. Jang, S. M. Lee, D. Yoo, T. J. Shin, J. H. Oh, C. Yang, *ACS Appl. Mater. Interfaces* **2014**, *6*, 20390; b) H. Zhou, L. Yang, A. C. Stuart, S. C. Price, S. Liu, W. You, *Angew. Chem.* **2011**, *123*, 3051; c) D. J. Crouch, D. Sparrowe, M. Heeney, I. McCulloch, P. J. Skabara, *Macromol. Chem. Phys.* **2010**, *211*, 2642.

[10] K. Neumann, C. Schwarz, A. Köhler, M. Thelakkat, *J. Phys. Chem. C* **2014**, *118*, 27.

[11] a) N. E. Jackson, B. M. Savoie, K. L. Kohlstedt, M. Olvera de la Cruz, G. C. Schatz, L. X. Chen, M. A. Ratner, *J. Am. Chem. Soc.* **2013**, *135*, 10475; b) H. J. Spencer, P. J. Skabara, M. Giles, I. McCulloch, S. J. Coles, M. B. Hursthouse, *J. Mater. Chem.* **2005**, *15*, 4783.

[12] a) L. Chen, D. Deng, Y. Nan, M. Shi, P. K. L. Chan, H. Chen, *J. Phys. Chem. C* **2011**, *115*, 11282; b) S.-Y. Liu, H.-Y. Li, M.-M. Shi, H. Jiang, X.-L. Hu, W.-Q. Li, L. Fu, H.-Z. Chen, *Macromolecules* **2012**, *45*, 9004.

[13] C. Kanimozhi, M. Naik, N. Yaacobi-Gross, E. K. Burnett, A. L. Briseno, T. D. Anthopoulos, S. Patil, *J. Phys. Chem. C* **2014**, *118*, 11536.

[14] B. Sun, W. Hong, Z. Yan, H. Aziz, Y. Li, *Adv. Mater.* **2014**, *26*, 2636.

[15] a) J. W. Jo, S. Bae, F. Liu, T. P. Russell, W. H. Jo, *Adv. Funct. Mater.* **2015**, *25*, 120; b) Z. Fei, M. Shahid, N. Yaacobi-Gross, S. Rossbauer, H. Zhong, S. E. Watkins, T. D. Anthopoulos, M. Heeney, *Chem. Commun.* **2012**, *48*, 11130; c) J. W. Jo, J. W. Jung, H.-W. Wang, P. Kim, T. P. Russell, W. H. Jo, *Chem. Mater.* **2014**, *26*, 4214.

[16] a) C.-H. Chen, Y.-J. Cheng, C.-Y. Chang, C.-S. Hsu, *Macromolecules* **2011**, *44*, 8415; b) Y.-J. Cheng, C.-H. Chen, Y.-S. Lin, C.-Y. Chang, C.-S. Hsu, *Chem. Mater.* **2011**, *23*, 5068; c) Y. X. Xu, C. C. Chueh, H. L. Yip, F. Z. Ding, Y. X. Li, C. Z. Li, X. Li, W. C. Chen, A. K. Jen, *Adv. Mater.* **2012**, *24*, 6356.

[17] M.-F. Falzon, A. P. Zoombelt, M. M. Wienk, R. A. J. Janssen, *Phys. Chem. Chem. Phys.* **2011**, *13*, 8931.

[18] A. K. Palai, S. P. Mishra, A. Kumar, R. Srivastava, M. N. Kamalasanan, M. Patri, *Macromol. Chem. Phys.* **2010**, *211*, 1043.

[19] A. C. Rochat, L. Cassar, A. Iqbal (CIBA-GEIGY Corp.), *Europe Patent 9, 4911*, **1983**.

[20] a) M. Vala, J. Vyňuchal, P. Toman, M. Weiter, S. Luňák Jr., *Dyes Pigm.* **2010**, *84*, 176; b) M. Vala, M. Weiter, J. Vyňuchal, P. Toman, S. Luňák, *J. Fluoresc.* **2008**, *18*, 1181.

[21] a) R. M. Osuna, R. P. Ortiz, M. C. Ruiz Delgado, Y. Sakamoto, T. Suzuki, V. Hernández, J. T. López Navarrete, *J. Phys. Chem. B* **2005**, *109*, 20737; b) Y. Sakamoto, S. Komatsu, T. Suzuki, *J. Am. Chem. Soc.* **2001**, *123*, 4643.

[22] B. Carsten, F. He, H. J. Son, T. Xu, L. Yu, *Chem. Rev.* **2011**, *111*, 1493.

[23] a) B. S. Nehls, U. Asawapirom, S. Füldner, E. Preis, T. Farrell, U. Scherf, *Adv. Funct. Mater.* **2004**, *14*, 352; b) H. Bronstein, Z. Chen, R. S. Ashraf, W. Zhang, J. Du, J. R. Durrant, P. Shakya Tuladhar, K. Song, S. E. Watkins, Y. Geerts, M. M. Wienk, R. A. J. Janssen, T. Anthopoulos, H. Sirringhaus, M. Heeney, I. McCulloch, *J. Am. Chem. Soc.* **2011**, *133*, 3272.

[24] a) K. Gräf, M. A. Rahim, S. Das, M. Thelakkat, *Dyes Pigm.* **2013**, *99*, 1101; b) C. M. Cardona, W. Li, A. E. Kaifer, D. Stockdale, G. C. Bazan, *Adv. Mater.* **2011**, *23*, 2367.

[25] J.-L. Bredas, *Mater. Horiz.* **2014**, *1*, 17.

[26] K. H. Hendriks, W. Li, M. M. Wienk, R. A. Janssen, *J. Am. Chem. Soc.* **2014**, *136*, 12130.

[27] F. Liu, C. Wang, J. K. Baral, L. Zhang, J. J. Watkins, A. L. Briseno, T. P. Russell, *J. Am. Chem. Soc.* **2013**, *135*, 19248.

[28] P. N. Murgatroyd, *J. Phys. D: Appl. Phys.* **1970**, *3*, 151.
[29] N. F. Mott, R. W. Gurney, *Electronic Processes in Ionic Crystals*, The Clarendon Press, Oxford, UK **1940**.
[30] C. Tanase, P. Blom, D. de Leeuw, *Phys. Rev. B* **2004**, *70*, 193202.
[31] Z. Chiguvare, V. Dyakonov, *Phys. Rev. B* **2004**, *70*, 235207.
[32] L. J. A. Koster, *Phys. Rev. B* **2010**, *81*, 205318.
[33] J. C. Blakesley, F. A. Castro, W. Kylberg, G. F. A. Dibb, C. Arantes, R. Valaski, M. Cremona, J. S. Kim, J.-S. Kim, *Org. Electron.* **2014**, *15*, 1263.
[34] R. Steyrleuthner, M. Schubert, F. Jaiser, J. C. Blakesley, Z. Chen, A. Facchetti, D. Neher, *Adv. Mater.* **2010**, *22*, 2799.
[35] M. A. Muth, W. Mitchell, S. Tierney, T. A. Lada, X. Xue, H. Richter, M. Carrasco-Orozco, M. Thelakkat, *Nanotechnology* **2013**, *24*, 484001.
[36] M. R. Lilliedal, A. J. Medford, M. V. Madsen, K. Norrman, F. C. Krebs, *Sol. Energy Mater. Sol. Cells* **2010**, *94*, 2018.
[37] S. Braun, W. R. Salaneck, M. Fahlman, *Adv. Mater.* **2009**, *21*, 1450.